Achieving Wider Bandwidth with Full-Wavelength Dipoles (FWDs) for 5G Base Stations

Can Ding, *Member, IEEE*, Hai-Han Sun, *Student Member, IEEE*, He Zhu, *Member, IEEE* and Y. Jay Guo, *Fellow, IEEE*

***Abstract*—A new method of designing full-wavelength dipoles (FWDs) is presented. A dual-polarized antenna is build based on FWDs for base station applications as an example. The antenna has four FWDs arranged in a square loop array form. The employed FWDs are bend upward to maintain a small aperture size, so that the realized element still fits in traditional base station antenna (BSA) array. The antenna is first matched across the band from 1.63 to 3.71 GHz, which can cover both the LTE band from 1.7 to 2.7 GHz and the 5G (sub-6 GHz) band from 3.3 to 3.6 GHz simultaneously. Then, band-stop filters are inserted in the feed networks of the antenna to suppress the radiation between 2.7 to 3.3 GHz. The antenna is fabricated and tested. Experimental results validate the simulation results. Comparing with the previously available FWD that has a bandwidth of 32%, the FWD proposed in this paper exhibits a much wider bandwidth of 78%. Moreover, this bandwidth is also comparable to and wider than those of the state-of-the-art BSAs based on half-wavelength dipoles (HWDs). The bandwidth enhancement and footprint reduction of the FWD in this work demonstrate a high potential of FWDs to be used in other applications.**

***Index Terms*—5G, base station antenna (BSA), dual-polarization, feed network, filter, full-wavelength dipole (FWD), sub-6 GHz band, wideband.**

I. Introduction

DIPOLE antennas are the simplest and most widely used class of antennas in radio communications. Based on the length of the dipole, it can be generally classified into three categories, i.e., short dipole, half-wavelength dipole (HWD), and full-wavelength dipole (FWD). A short dipole has its total length less than a tenth of a wavelength [1, 2]. Due to its small size, its feed point impedance includes a large capacitive reactance and a small resistance, thereby leading to a narrow bandwidth. It is usually used in applications where size is the main concern. A HWD has a total length approximately half a wavelength. At the center frequency, the dipole has a zero reactance and is said to be resonant. HWD is the most common type of dipoles used in various applications thanks to its simple configuration and balanced performance, i.e., bandwidth and directivity. FWD, as implied in its name, has a length of approximately a wavelength at the center frequency, where anti-resonance occurs and the reactance is also zero. However, unlike short dipoles and HWDs that are widely used, FWDs are seldom used in industry despite their higher directivity. This is largely due to a misconception that FWD is difficult to feed and the bandwidth is narrow.

Indeed, in the early days, matching and feeding of FWD were quite difficult. There were only a few publications in the literature discussing offset feedings [3, 4] and dual/triple feedings [5–7] for FWDs. All these methods suffer from high complexity and result in narrow bandwidth, thus did not promote FWD in real applications. In [8], a patch antenna utilized both the fundamental mode and the first even-order mode, which is the full-wavelength mode, to enhance the bandwidth of the radiation (25%). However, this method is difficult to be used on dipole antennas. In 2017, another method of matching FWDs was proposed in [9]. In this work, instead of matching a single FWD, four FWDs were connected in parallel so that the high resistance of FWD can be reduced to facilitate the impedance matching. Recently, a simple yet wideband center feeding method for FWD was developed [10]. With the very standard dipole configuration, i.e., two linear, straight conductor arms, the FWD was successfully matched across a fractional bandwidth of 32%. It also demonstrated that the FWD potentially exhibits more bandwidth than a HWD with a similar standard configuration. In order to broaden the application of FWDs, however, one would need to reduce the size of FWDs and to improve the antenna bandwidth much further.

In this work, a dual-polarized base station antenna (BSA) is presented based on FWDs to demonstrate their wide bandwidth and footprint reduction potentials. The cellular base station application is selected as the platform to demonstrate the superiority of FWD for the following reasons. Firstly, BSA is one of the most important applications where HWD is extensively used [11–27]. HWDs are robust, low cost, easy to realize dual-polarization, and they exhibit better performance than BSAs based on patches [28] and waveguides [29]. Second, antennas of much wider bandwidth are now in demand for BSAs. In the upcoming 5G era, more frequency bands will be utilized, including the sub-6 GHz bands (3.55-3.7 GHz in USA, 3.4-3.8 GHz in Europe, 3.3-3.6 GHz in China) as well as the mm-wave bands (24-28 GHz, 37-40 GHz) [30]. While the new BSAs covering the mm-wave bands will be implemented in a separate platform, BSAs covering the sub-6 GHz band are very likely to be integrated with the existing 3G/4G BSAs covering 1.71-2.69 GHz band to minimize the overall cost. Therefore, a wide band antenna that is capable of covering 3G/4G/5G (sub-6 GHz) bands simultaneously is a competitive candidate for future 3G/4G/5G co-existing systems.

Modern BSAs require dual-polarization to combat the mul-

Manuscript submitted 05 Apr. 2019; revised 25 Jun. 2019; accepted 21 Jul. 2019. This work was funded by Australian Research Council (ARC) DP160102219. (*Corresponding author: Can Ding*)

All the authors are with the Global Big Data Technologies Centre (GBDTC), the University of Technology Sydney (UTS), Ultimo, NSW, 2007, Australia. e-mail:(can.ding.1989@gmail.com)

tipath effect. In this work, four FWDs are employed and arranged in a tightly-coupled square loop array configuration. By exciting the FWDs simultaneously in two different ways, the required dual-polarization is attained. The antenna is optimized to meet BSA specifications. On one hand, the aperture size of the antenna is comparable with state-of-the-art BSAs [21–27] employing HWDs and it still fits in the currently used 3G/4G arrays. On the other hand, the modification of the FWDs does not change the essence of FWD, thereby the attained antenna has a wide bandwidth of 77% from 1.63 to 3.71 GHz, which covers the 3G/4G bands (1.7-2.7 GHz) and the 5G band (3.3-3.6 GHz) simultaneously for future co-existing 3G/4G/5G antenna systems.

The remaining of the paper is organized as follows. Following the introduction, Section II presents the antenna design and Section III describes the antenna fabrication and test results. Finally, the paper is concluded in Section IV.

II. Antenna Design

A. Antenna aperture

Fig. 1 shows the thought process for creating the proposed antenna configuration. Note that the feed networks are not considered here since they have minor effects on the radiation pattern, and all the radiators are excited by ideal discrete ports for simplicity. Fig. 2 plots the half-power-beamwidth (HPBW) of the radiation patterns of each configuration. For typical three-sector BSAs, whether the antenna has a stable radiation pattern, i.e., HPBW is around 65° in the horizontal plane across the frequency band, is a widely used performance specification [12].

As shown in Fig. 1, Configuration 1 is a tightly-coupled HWD square loop array BSA advocated in [16]. It consists of four HWDs arranged in a square loop. With proper excitation, the radiation of the four HWDs combines into the required pattern for 3G/4G base station systems. The HPBW of the antenna in the horizontal plane, i.e., *x*-*z* plane, is shown in Fig. 2. Across the 3G/4G band, i.e., 1.7-2.7 GHz, the HPBW is very stable and can meet the requirement for cellular coverage. However, with the frequency increasing, the HPBW increases dramatically when $f > 3.3$ GHz.

Configuration 2 has a similar configuration as Configuration 1 but the radiators are replaced by FWDs. Although employing FWDs might enhance the bandwidth, this configuration has much larger aperture size, which can cause troubles when used in arrays. Moreover, as shown in Fig. 2, the HPBW is too narrow for cellular coverage.

To avoid the large aperture size so that the antenna still fits in the standard BSA array panel, Configuration 3 has the ends of each FWD bend upward. Similar to that of Configuration 1, the attained HPBW is relatively stable across 3G/4G band but gets wider at the higher 5G band. To flatten the variation of HPBW, Configuration 4 has a circular director placed atop the aperture to narrow the HPBW at higher frequencies. As shown in Fig. 2, the HPBW of Configuration 4 is maintained very stable, i.e., 61° ± 3°, across the entire band from 1.7 to 3.6 GHz. Therefore, to guarantee the stable radiation pattern across the sub-6 GHz bands, we selected configuration 4 to commence the design.

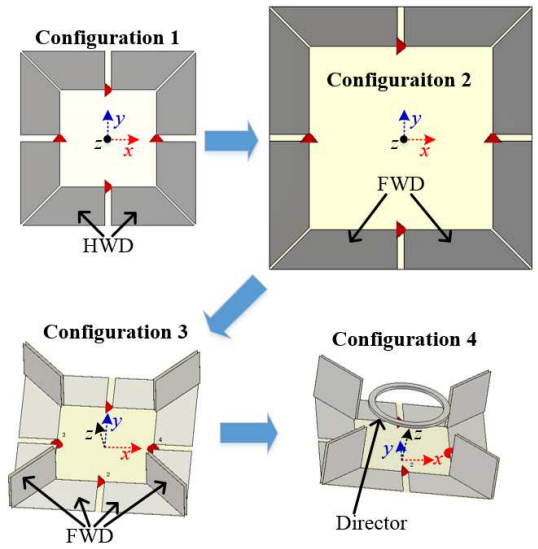

Fig. 1. Antenna structure evolvement. Configuration 1: Square loop array employing four HWDs. Configuration 2: Square loop array employing four FWDs. Configuration 3: Square loop array employing four FWDs with edges bend upward. Configuration 4: Square loop array employing four FWDs with bend edges and a director.

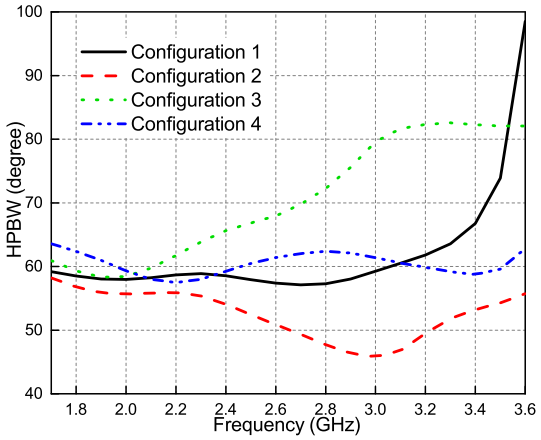

Fig. 2. Simulated HPBWs in the horizontal plane (*y*-*z* plane) of Configurations 1, 2, 3, and 4 shown in Fig. 1 across the band from 1.7 to 3.6 GHz.

The input impedance seen from the ideal discrete ports is plotted in Smith chart as shown Fig. 3. Note that the impedances of the four ideal ports are identical. As observed in the Smith chart, the impedance rotates in clockwise direction with the frequency increasing, intersecting with the zero reactance line at $f = 1.96$ GHz when anti-resonance occurs, which is a typical FWD behavior. This demonstrates that bending the FWDs and putting the FWDs close to each other to enhance the mutual coupling do not change the essence of FWD.

B. Antenna impedance matching with filter-based circuit

A FWD having anti-resonance at the center frequency can be seen as a resistor in parallel with a shunt L-C circuit. As shown in Fig. 3, the resistance is large and the reactance changes rapidly with frequency, which makes a FWD difficult to match. As suggested in [10], FWD can be matched across

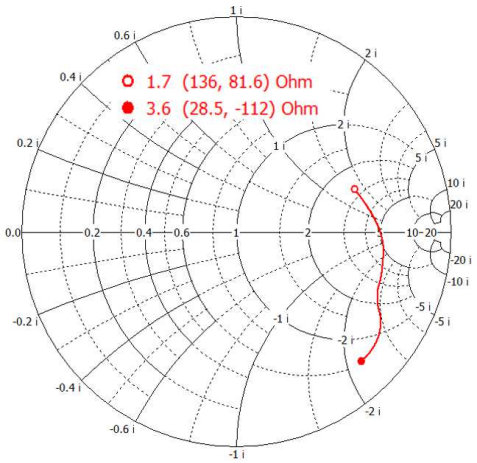

Fig. 3. Input impedance of each FWD in the square loop array.

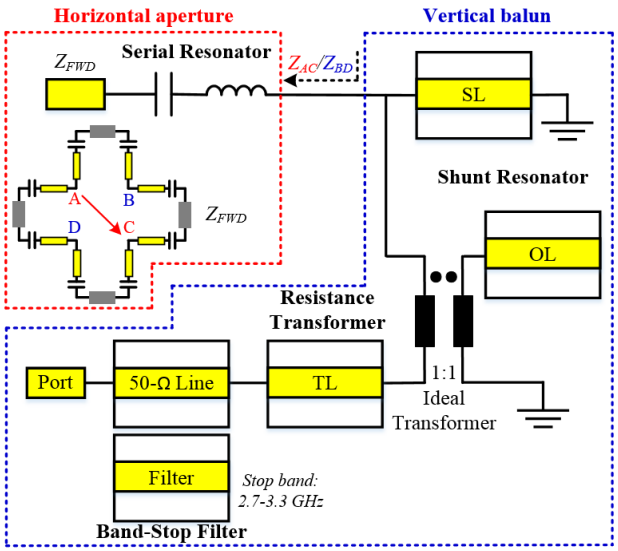

Fig. 4. Circuit theory model of the matching circuit.

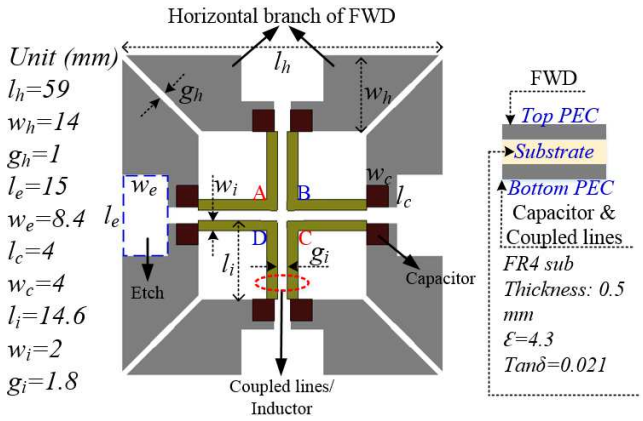

(a)

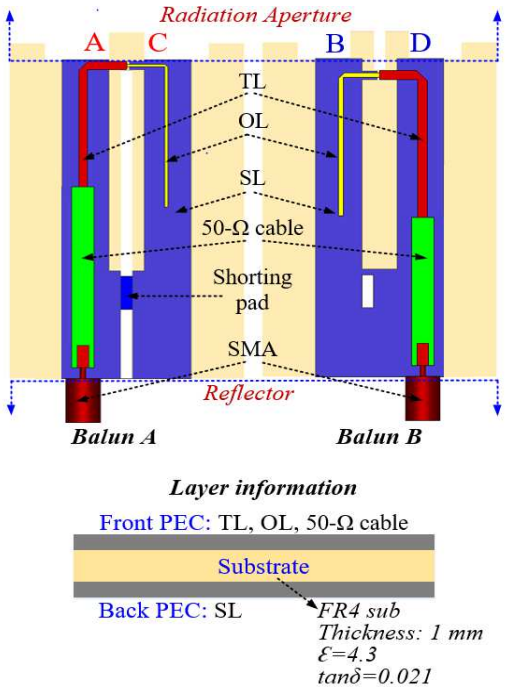

(b)

Fig. 5. Physical implementation of the matching circuit. (a) Perspective view of the horizontal aperture. Note that the director and the vertical branches of the FWDs are hidden for clarity. (b) Perspective view of the vertical baluns.

a reasonable band (32%) using a filter-based matching circuit. However, matching the antenna proposed in this work is challenging because we need to excite four FWDs simultaneously and the target bandwidth is much wider (78%).

A circuit theory model of the filter-based matching circuit for the proposed antenna is shown in Fig. 4. The matching circuit is partly implemented on the radiation aperture placed horizontally and partly implemented on a vertical printed circuit board (PCB) in perpendicular with the horizontal aperture, as shown in Figs. 5(a) and 5(b), respectively.

Overall speaking, the antenna proposed in this work is matched by a band-pass filter to mitigate the variation of the reactance, and a resistance transformer to transfer the high resistance back to 50-Ω across the target band. The equivalent circuit of the FWD itself contains a shunt resonator, which is the first stage of the filter. Two tuners, i.e., a serial resonator and a shunt resonator, are introduced in the matching circuit to form a three-stage band-pass filter, as shown in Fig. 4. Followed by the band-pass filter, the third tuner is a quasi-quarter-wavelength transmission line (TL) used to tune the resistance. The additional band-stop filter shown in the figure is not compulsory for impedance matching and it will be discussed in the next subsection.

Since the proposed antenna consists four FWDs and they are excited simultaneously, all of the FWDs need to be matched. A straightforward solution is to replicate the matching circuit for one FWD by four; but this will occupy an unacceptable size. Instead of replicating all the matching components, only the serial resonator is replicated by four while the other components remain the same.

As shown in Fig. 5(a), there are four FWDs and four pairs of serial LC resonators on the horizontal aperture. The capacitances are provided by the parallel plate capacitors formed by FWD printed on the front side and small piece of metallic pads ($w_c \times l_c$) printed on the back side of the horizontal PCB. The inductances are provided by the coupled lines with

high characteristic impedance, which are also printed on the back side of the horizontal PCB. Note that for each FWD, two serial LC resonators are employed to maintain the balance and there are eight serial resonators in total. In addition, as shown in Fig. 5(a), a rectangular pad ($w_e \times l_e$) is etched on each FWD to avoid unwanted resonating mode that deteriorates the radiation pattern.

As indicated in the red box of Fig. 4, by placing a differential voltage across AC or BD, all the four FWDs are excited and $-45°$ or $+45°$-polarized radiation is generated, respectively. The four pairs of LC resonators transfer the input impedance Z_{FWD} to Z_{AC}/Z_{BD}. The impedances $Z_{AB} = Z_{BC} = Z_{CD} = Z_{DA}$ are equal to the input impedance of the dipole in series with the serial resonator, i.e., Z_{FWD+SR}. According to the schematic diagram of the dipole connection, the impedances

$$\begin{aligned} Z_{AC} &= (Z_{AB} + Z_{BC})//(Z_{AD} + Z_{DC}) = Z_{FWD+SR}, \\ Z_{BD} &= (Z_{BC} + Z_{CD})//(Z_{BA} + Z_{AD}) = Z_{FWD+SR}. \end{aligned} \quad (1)$$

Therefore, matching the impedances Z_{AC} or Z_{BD} is equivalent to matching Z_{FWD+SR}.

The circuit to match Z_{FWD+SR} (Z_{AC} or Z_{BD}) is shown in the blue box in Fig. 4 and is implemented on the vertical PCB as shown in Fig. 5(b). Since a FWD at its anti-resonance can be modelled by a shunt LC resonator, which works as the first stage of ladder-type band-pass filter, and the second stage, i.e., the serial LC resonator, is also included in Z_{FWD+SR}, we only need one more shunt resonator acting as the third stage to complete the band-pass filter design. The shunt resonator is realized by a coupled line shorted to the ground (SL), i.e., the main part of balun, and an open transmission line (OL). SL and OL are implemented on the back and front sides of the vertical PCB as shown in Fig. 5(b). The 1:1 transformer represents the coupling between the microstrip lines and the coupled lines printed on the two sides of the substrate. Following the shunt resonator is the resistance transformer realized by a quasi-quarter-wavelength microstrip line near the center frequency.

We remark that the optimization was firstly conducted based on the circuit model shown in Fig. 4 in a circuit theory simulation environment as it is much faster than that in a full-wave simulation environment. Once the initial values were determined, a physical model was then constructed in a full-wave simulation software, as shown in Fig. 6. In this work, all the simulations were conducted in CST Microwave Studio 2017 as it contains both a circuit-theory simulation module and a full-wave simulation module.

The optimized dimension values of the feed networks are listed in Table I. Fig. 7 plots the simulated reflection coefficients and HPBW at the two ports of the antenna. Note that the results are obtained without the extra filters. It is shown that, with the optimized matching networks, the antenna has a wide impedance bandwidth, i.e., from 1.63 to 3.71 GHz with a fractional bandwidth of 78%, for both the two polarizations. Compared to the FWD with a standard configuration having a bandwidth of 32% [10], the achieved bandwidth by the FWDs with tightly-coupled square loop configuration is significantly wider. Moreover, the achieved bandwidth is also wider than the comparable tightly-coupled HWD square loop arrays which

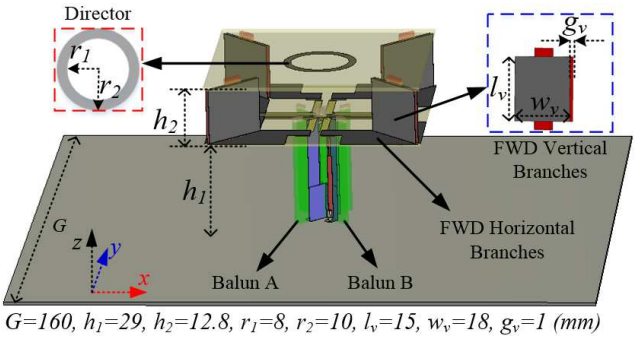

Fig. 6. Perspective view of the resultant tightly-coupled FWD square loop array.

TABLE I
DIMENSIONS OF THE FEED NETWORKS (IN MILLIMETERS)

Parameter	Feed A	Feed B	Description
L_SL	19.2	14.4	Length of SL
g_SL	3	3	Width of the gap between SLs
L_OL	16.04	15.7	Length of OL
W_OL	0.23	0.4	Width of OL
L_TL	14	15.86	Length of TL
W_TL	0.75	0.82	Width of TL
L_cable	16.46	13.49	Length of the 50-Ω cable
W_cable	1.94	1.94	Width of the 50-Ω cable
L_filter	13.3	13.49	Length of the filter line
W_filter	1.3	1	Width of the filter line
g_filter	0.3	0.3	Distance between the filter and the 50-Ω cable

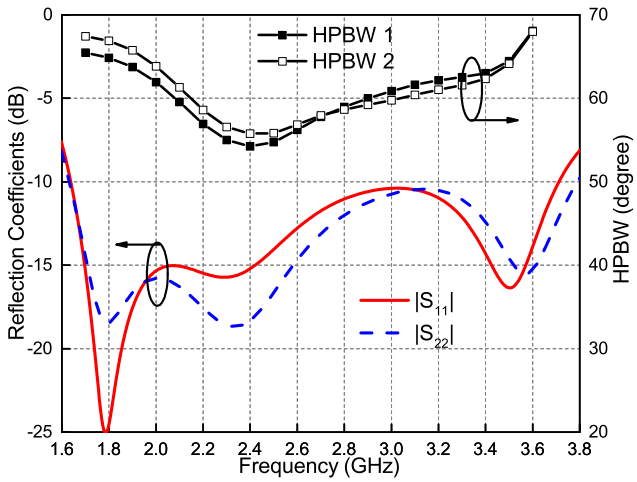

Fig. 7. Simulated reflection coefficients and HPBWs at the two ports of the tightly-coupled FWD square loop array antenna.

usually have the bandwidth of 45% [16, 31]. Even compared with the state-of-the-art base station antennas [21–27], this bandwidth is comparable or wider. Meanwhile, the HPBWs are very stable across the target band from 1.7 to 3.6 GHz.

C. Additional band-stop filter

The obtained antenna has an impedance bandwidth from 1.63 to 3.71 GHz, which well covers both the 3G/4G and 5G cellular bands, i.e., 1.71-2.69 GHz and 3.3-3.6 GHz. However, the radiation in the spectrum in-between is unwanted.

This article has been accepted for publication in a future issue of this journal, but has not been fully edited. Content may change prior to final publication. Citation information: DOI 10.1109/TAP.2019.2950108, IEEE Transactions on Antennas and Propagation

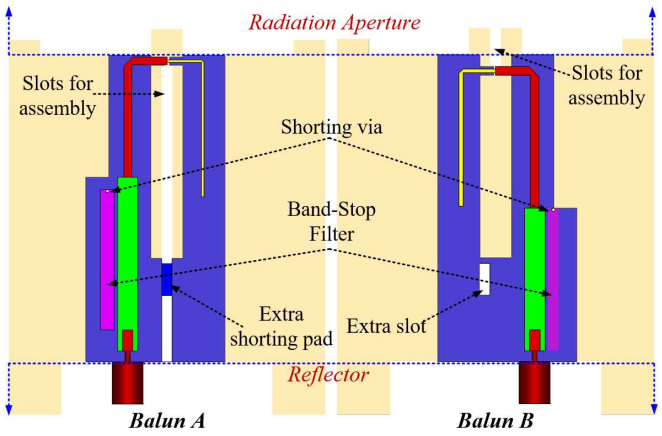

Fig. 8. Perspective view of the vertical baluns with additional band-stop filters.

Therefore, like some filtering antennas [32–34], to make this antenna more practical for the 3G/4G/5G co-existing system, a band-stop filter is inserted at the end of each matching circuit to suppress the radiation between the two bands. As shown in Fig. 8, the additional band-stop filters are implemented using additional microtrip lines coupled with the 50-Ω cable lines. The dimensions of the optimized filters are also listed in Table I. Note that the filters are designed on the basis of the attained antenna shown in Fig. 6. The dimensions of the other parts of the feed networks are unchanged. We remark that the pass-band and stop-band performance can be further improved by conducting an overall optimization considering both the filter design and the matching circuit.

Usually, the required band-stop filters are included in the TR module attached under the reflector of a base station array. In this work, the feed network is designed to have an ability to suppress the radiation across the unwanted band, which can take some loads from the TR module and lower the cost of the entire system.

Figs. 9(a) and 9(b) compare the reflection coefficients and transmission coefficients, respectively, at the two ports of the antenna with and without the extra band-stop filters. As shown in Fig. 9(a), by adding extra band-stop filters, noticeable notches between 2.8 and 3.3 GHz are attained without deteriorating the impedance matching across the two useful bands (1.7-2.7 GHz, 3.3-3.6 GHz). Meanwhile, as observed from Fig. 9(b), the extra band-stop filters only introduce small changes to the transmission coefficients between the two ports. With or without the filters, the $|S_{12}|$ remains to be < -28 dB.

Although the band stop performance resulting from the filters is not excellent, the cost of achieving the notches is simply two additional microstrip lines coupling with the feed lines. Here we claim that, with the proper matching technique, the size of the feed networks can be minimized and the saved space can be used for other purposes. For example, in this work, a band-stop filter is inserted to each of the feed network, which could release the load of the filters in the T/R module. Moreover, as shown in Fig. 5(b), the 50-Ω cables and filters in the feed networks can be replaced by phase shifters, amplifiers, couplers [35], or other components to achieve other functionalities for different applications.

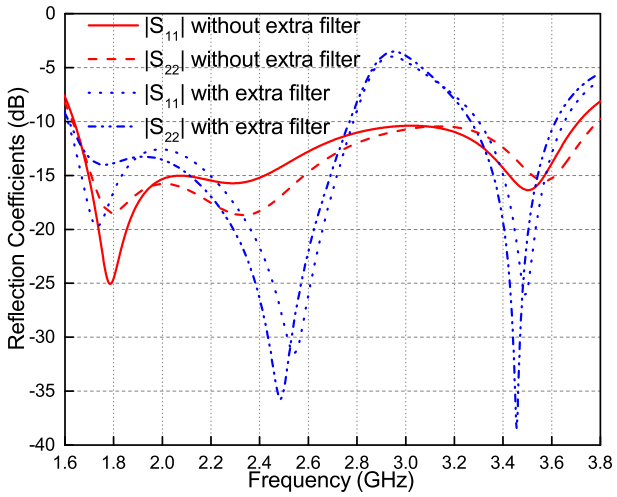

(a)

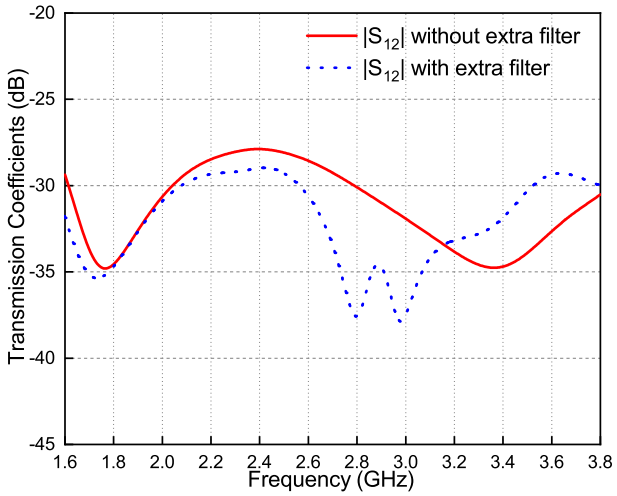

(b)

Fig. 9. Simulated (a) reflection coefficients and (b) transmission coefficients at the two ports of the tightly-coupled FWD square loop array antenna with and without the band-stop filters.

III. Fabrication and Test

A. Antenna fabrication

Fig. 10(a) shows a disassembled view of the final antenna model ready for fabrication. As shown in the figure, the antenna can be divided into six components, including five PCB designs and one metal ground. These parts were fabricated separately and assembled thereafter. In this work, the metal ground was made by an aluminum board with a thickness of 1 mm. The substrate of the PCBs is FR4 with ε = 4.3 and $tan\delta$ = 0.021. The thicknesses of PCB 3 and all the other PCBs are 0.5 mm and 1 mm, respectively. All the PCBs have metal printed on their both sides and the metal areas are highlighted in dark red color in Fig. 10(a). Details of the metal patterns on the PCBs are illustrated in Figs. 5, 6, and 8. Tab-and-slot structures are designed on each component to facilitate the assembly.

This article has been accepted for publication in a future issue of this journal, but has not been fully edited. Content may change prior to final publication. Citation information: DOI 10.1109/TAP.2019.2950108, IEEE Transactions on Antennas and Propagation

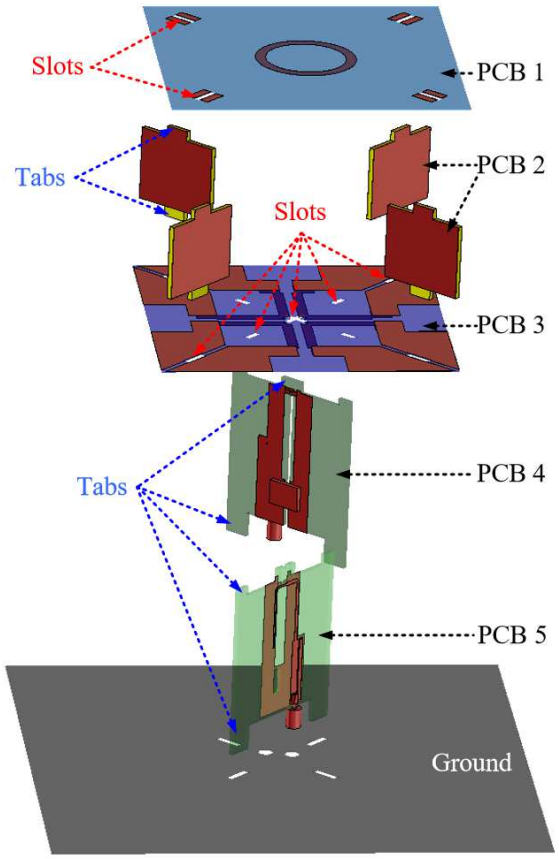

(a)

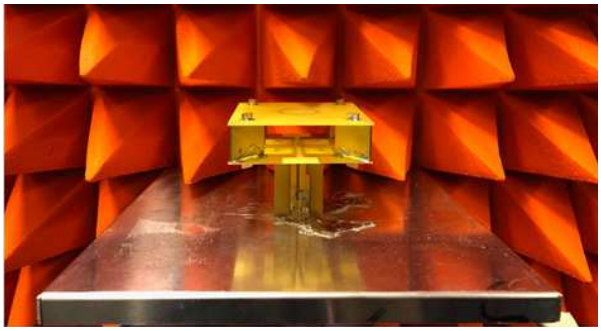

(b)

Fig. 10. (a) Disassembled view of the antenna configuration. (b) Photo of the fabricated antenna prototype.

The specific assembly procedure is as follows. First, thanks to the properly designed slots on the baluns (details of the layouts are shown in Fig. 8), PCBs 4 and 5 were plugged together perpendicularly, forming into an inter-crossing balun (PCB 4+5). Note that the slot etched on balun A (PCB 4) used for assembly breaks the balun, which can deteriorate the matching performance. Therefore, to ensure a good shorting for balun A, after the two baluns were plugged together, an extra shorting pad was inserted into the extra slot on Balun B, as shown in Fig. 8. Then the substrate tabs designed on PCBs 2, 4, and 5 were inserted into the corresponding slots etched on PCBs 1 and 3, as shown in Fig. 10(a). The components were fixed together by soldering, i.e., PCBs 1 and 2 were fixed together by soldering the top tabs of PCB 2 onto the

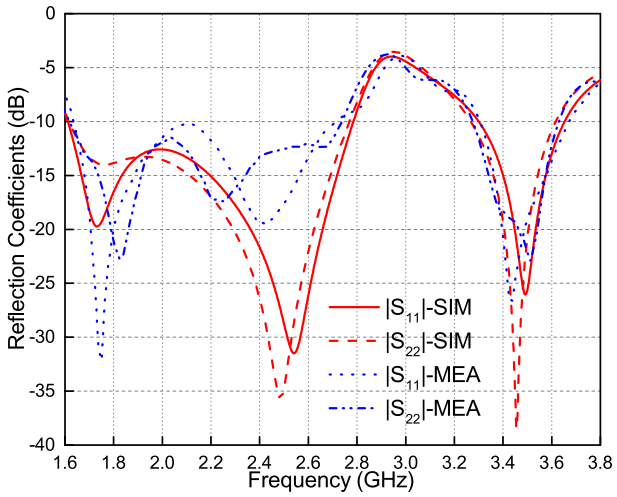

(a)

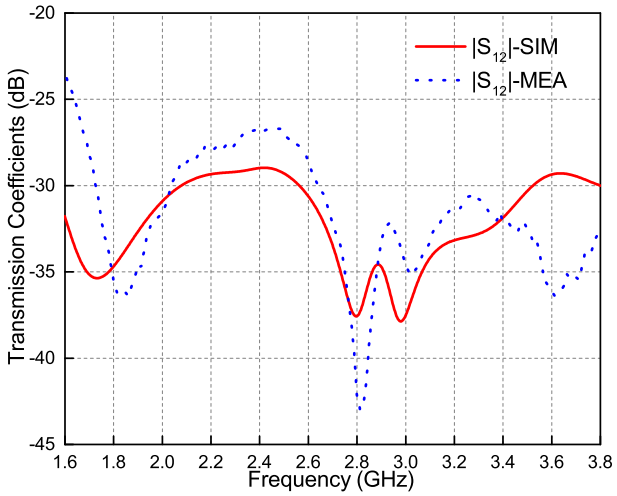

(b)

Fig. 11. Simulated and measured (a) reflection coefficients and (b) transmission coefficients of the dual-polarized square loop antenna array employing four FWDs.

small pieces of metal on the top side of PCB 1; PCBs 2 and 3 were fixed together by soldering the vertical dipole branches on PCB 2 onto the horizontal dipole branches printed on the top side of PCB 3; PCBs 3 and 4+5 were fixed by soldering the top of SLs on the baluns (PCBs 4+5) onto the coupled lines printed on the backside of PCB 3. Finally, the assembled antenna model was plugged into and soldered onto the metal ground. A photo of the attained antenna prototype is shown in Fig. 10(b).

B. Test results

The obtained antenna prototype was also tested. The simulated and measured reflection and transmission coefficients of the two polarizations are plotted in Figs. 11(a) and 11(b), respectively. It is observed that the measured results agree well with the simulated ones. According to the measurement results, the reflection coefficients for both the two polarizations are < -10 dB and the isolation between the two ports are < -28

This article has been accepted for publication in a future issue of this journal, but has not been fully edited. Content may change prior to final publication. Citation information: DOI 10.1109/TAP.2019.2950108, IEEE Transactions on Antennas and Propagation

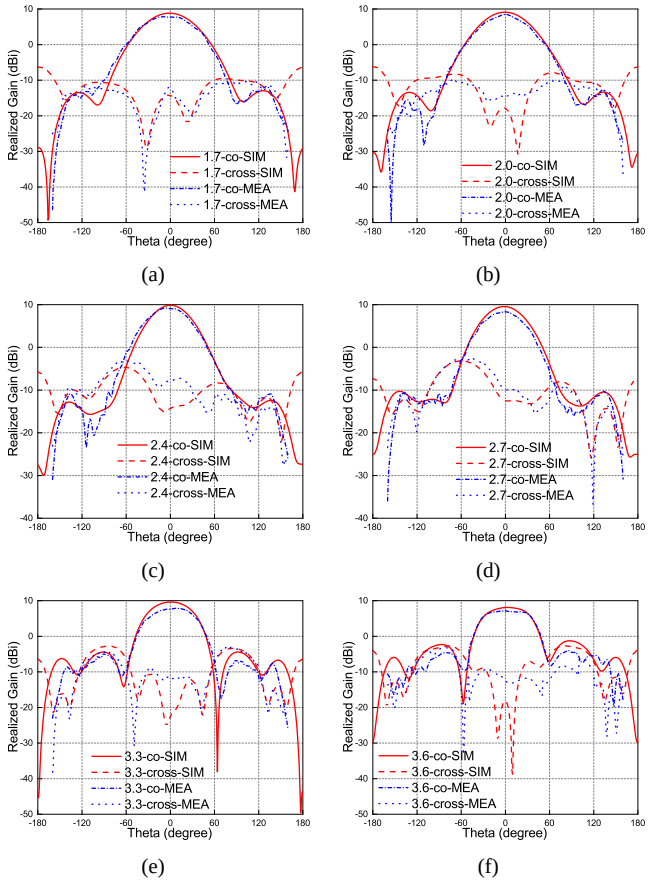

Fig. 12. Simulated and measured co- and cross-polarization radiation patterns in the horizontal plane (*x*-*z* plane) of the +45°-polarized antenna at 1.7, 2.0, 2.4, 2.7, 3.3, and 3.6 GHz.

dB across the two target bands, i.e., 1.7-2.7 GHz and 3.3-3.6 GHz.

The radiation performance of the antenna was measured in the anechoic chamber at Data61, CSIRO, located in Marsfield, Australia. The simulated and measured co- and cross-polarization patterns in the horizontal plane (*x*-*z* plane) of the +45°-polarized antenna are shown in Fig. 12. Note that only the patterns for one polarization is shown here since the results for the other polarization are necessarily the same due to the symmetry of the radiation aperture. Six frequency samples within the two operational bands were selected. As illustrated in the figure, the measured results agree well with the simulated ones and variations of the patterns across the two bands are minor.

Fig. 13 gives the simulated and measured realized gains of the dual-polarized antenna with band-stop filters in its feed networks. In addition, the simulated realized gains of the antenna without band-stop filter are also included in the figure for comparison. As illustrated in the figure, the antenna gain across the band from 2.8 to 3.2 GHz has been noticeably reduced due to presence of the filters. The measured gains agree necessarily well with the simulated ones at frequencies when $f < 2.9$ GHz. At higher frequencies when $f > 2.9$ GHz, the measured gains are lower than the simulated results. This is due to the fact that the used coaxial cables in the measurement, i.e., ENVIROFLEX_316 from Huber+Suhner [36], are designed to work under 3 GHz, which introduce additional losses at higher frequencies. The simulated efficiencies of the two polarizations have similar variation trends as the gain results, i.e., within the two operational bands, the efficiencies are quite stable (> 80%); within the unwanted spectrum in-between, the efficiencies are significantly reduced and reach to nearly 20% at 2.9 GHz. Moreover, the measured HPBWs of the antenna for both the two polarizations are within 58°-69° and 62°-69° across the 1.7-2.7 GHz and 3.3-3.6 GHz bands, respectively.

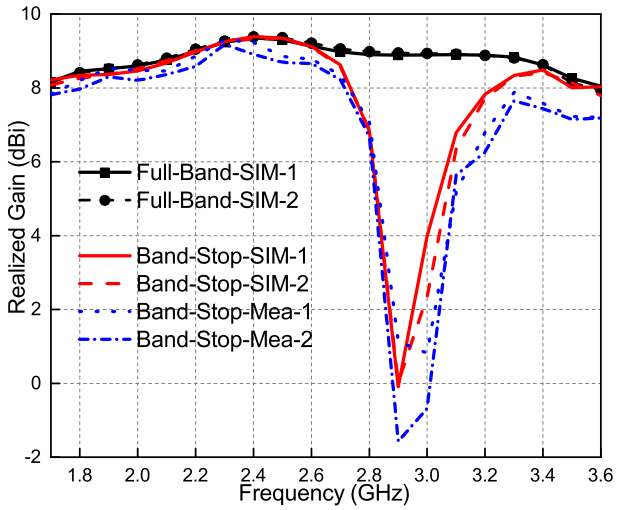

Fig. 13. Simulated and measured realized gains for the two polarizations of the final antenna and the simulated realized gains of the antenna without the band-stop filters.

IV. Conclusion

This paper promoted the practicality of FWDs by demonstrating the fact that the bandwidth of FWD can be significantly enhanced compared to the FWD with a standard configuration. A base station antenna employing four FWDs arranged in a square loop configuration was designed as an example. Using FWDs other than HWDs to design the antenna can lead to a larger size. However, in this work, the FWDs were modified to guarantee that the attained antenna has a similar aperture size compared to the state-of-the-art designs based on HWDs. Despite the aperture size is restricted, the impedance of the resultant antenna still has a typical FWD behavior and the FWD-based antenna was successfully matched across a wide fractional bandwidth of 78% from 1.63 to 3.71 GHz. This bandwidth is much wider than that of the similar configuration based on HWDs (around 45%) and is comparable to those of the state-of-the-art BSAs (around 70%). The method of enhancing the bandwidth and reducing the footprint size of FWD proposed is expected to be able to promote the use of FWDs in the antenna society. In addition, band-stop filters were embedded in the feed networks with minimum cost to suppress the radiation at the frequencies between 2.8-3.3 GHz. Therefore, the obtained antenna is able to operate at the 1.7-2.7 and 3.3-3.6 GHz bands simultaneously,

suitable for future 3G/4G/5G co-existing base station antenna systems.

V. Acknowledgement

The authors would like to sincerely thank their colleague Dr. Shulin Chen for his assistance with the antenna measurement.

References

[1] A. D. Yaghjian and H. R. Stuart, "Lower Bounds on the Q of Electrically Small Dipole Antennas," *IEEE Transactions on Antennas and Propagation*, vol. 58, no. 10, pp. 3114-3121, Oct. 2010.

[2] R. W. Ziolkowski and A. Erentok, "Metamaterial-based efficient electrically small antennas," *IEEE Transactions on Antennas and Propagation*, vol. 54, no. 7, pp. 2113-2130, July 2006.

[3] S. H. Idris and C. M. Hadzer, "Analysis of the radiation resistance and gain of a full-wave dipole," *IEEE Antennas and Propagation Magazine*, vol. 36, No. 5, pp. 45-47, Oct. 1994.

[4] H. Hosono, K. Shibata, K. Saegusa and T. Takano, "The radiation characteristics and current distribution of a full wavelength dipole," *2014 IEEE Antennas and Propagation Society International Symposium (APSURSI)*, Memphis, TN, pp. 75-76, 2014.

[5] K. A. Hmood, S. I. S. Hassan and M. F. Ain, "Design of dual feeding full-wave dipole antenna for VHF," *2006 International RF and Microwave Conference*, Putra Jaya, 2006, pp. 135-139.

[6] Y. Khraisat, K. Hmood and A. Anwar, "Analysis of the radiation resistance and gain of full-wave dipole antenna for different feeding design," *Journal of Electromagnetic Analysis and Applications*, vol. 4, no. 6, 2012, pp. 235-242.

[7] Y. Khraisat, K. Hmood and A. Anwar, "The current distribution of symmetrical dual and triple feeding full-wave dipole antenna," *Modern Applied Science*, vol. 5, no. 6, 2011, pp. 126-132.

[8] W. J. Lu, X. Q. Li, Q. Li, and L. Zhu, "Generalized design approach to compact wideband multi-resonant patch antennas," *International Journal of RF and Microwave Computer-Aided Engineering*, col. 28, no. 8, Oct. 2018.

[9] G. Sun, S. Wong and H. Wong, "A Broadband Antenna Array Using Full-Wave Dipole," *IEEE Access*, vol. 5, pp. 13054-13061, 2017.

[10] C. Ding, B. Jones, Y. J. Guo and P.-Y. Qin, "Wideband Matching of Full-Wavelength Dipole With Reflector for Base Station," *IEEE Transactions on Antennas and Propagation*, vol. 65, no. 10, Oct. 2017.

[11] B. B. Jones and J. K. A. Allan, "Ultra-Wideband Dual-Band Cellular Base Station Antenna," US Patent 2014/0139387 A1, May, 2014.

[12] C. Ding, H. H. Sun, R. W. Ziolkowski, and Y. J. Guo, "Simplified Tightly-Coupled Cross-Dipole Arrangement for Base Station Applications," *IEEE Access*, vol. 5, pp. 27491-27503, 2017.

[13] H. H. Sun, C. Ding, B. Jones, and Y. J. Guo, "A Wideband Base Station Antenna Element with Stable Radiation Pattern and Reduced Beam Squint," *IEEE Access*, vol. 5, pp. 23022-23031, 2017.

[14] Y. Cui, R. Li and H. Fu, "A Broadband Dual-Polarized Planar Antenna for 2G/3G/LTE Base Stations," *IEEE Transactions on Antennas and Propagation*, vol. 62, no. 9, pp. 4836-4840, Sept. 2014.

[15] Z. Bao, Z. Nie and X. Zong, "A Novel Broadband Dual-Polarization Antenna Utilizing Strong Mutual Coupling," *IEEE Transactions on Antennas and Propagation*, vol. 62, no. 1, pp. 450-454, Jan. 2014.

[16] C. Ding, H. Sun, R. W. Ziolkowski and Y. Jay Guo, "A Dual Layered Loop Array Antenna for Base Stations With Enhanced Cross-Polarization Discrimination," *IEEE Transactions on Antennas and Propagation*, vol. 66, no. 12, pp. 6975-6985, Dec. 2018.

[17] S. X. Ta, I. Park, and R. W. Ziolkowski, "Crossed Dipole Antennas: A review," *IEEE Antennas and Propagation Magazine*, vol. 57, no. 5, pp. 107-122, Oct. 2015.

[18] K. M. Luk and B. Wu, "The Magnetoelectric Dipole – A Wideband Antenna for Base Stations in Mobile Communications," *Proceedings of the IEEE*, vol. 100, no. 7, pp. 2297-2307, Jul. 2012.

[19] H. Huang, Y. Liu, and S. X. Gong, "A Novel Dual-Broadband, Dual-Polarized Antenna for 2G/3G/LTE Base Stations," *IEEE Transactions on Antennas and Propagation*, vol. 64, no.9, pp. 4113-4118, 2016.

[20] Y. Luo, Q. X. Chu and J. Bornemann, "Enhancing cross-polarisation discrimination or axial ratio beamwidth of diagonally dual or circularly polarised base station antennas by using vertical parasitic elements," *IET Microwaves, Antennas and Propagation*, vol. 11, no. 9, pp. 1190-1196, Jul. 2017.

[21] M. Li, Q. L. Li, B. Wang, C. F. Zhou and S. W. Cheung, "A Low-Profile Dual-Polarized Dipole Antenna Using Wideband AMC Reflector," *IEEE Transactions on Antennas and Propagation*, vol. 66, no. 5, pp. 2610-2615, May 2018.

[22] L. Wen et al., "A Wideband Dual-Polarized Antenna Using Shorted Dipoles," *IIEEE Access*, vol. 6, pp. 39725-39733, 2018.

[23] B. Feng, L. Li, Q. Zeng and C. Sim, "A Low-Profile Metamaterial Loaded Antenna Array With Anti-Interference and Polarization Reconfigurable Characteristics," *IEEE Access*, vol. 6, pp. 35578-35589, 2018.

[24] Q. Zhang and Y. Gao, "A Compact Broadband Dual-Polarized Antenna Array for Base Stations," *IEEE Antennas and Wireless Propagation Letters*, vol. 17, no. 6, pp. 1073-1076, Jun. 2018.

[25] Y. Cui, X. Gao, H. Fu, Q. Chu and R. Li, "Broadband Dual-Polarized Dual-Dipole Planar Antennas: Analysis, Design, and Application for Base Stations," *IEEE Antennas and Propagation Magazine*, vol. 59, no. 6, pp. 77-87, Dec. 2017.

[26] A. Alieldin et al., "A Triple-Band Dual-Polarized Indoor Base Station Antenna for 2G, 3G, 4G and Sub-6 GHz 5G Applications," *IEEE Access*, vol. 6, pp. 49209-49216, 2018.

[27] Y. Cui, L. Wu and R. Li, "Bandwidth Enhancement of a Broadband Dual-Polarized Antenna for 2G/3G/4G and IMT Base Stations," *IEEE Transactions on Antennas and Propagation*, vol. 66, no. 12, pp. 7368-7373, Dec. 2018.

[28] Y. Jin and Z. Du, "Broadband dual-polarized f-probe fed stacked patch antenna for base stations," *IEEE Antenna and Propagation Letter*, vol. 14, pp. 1121-1124, 2015.

[29] H. L. Zhu, K. L. Chung, C. Ding, G. Wei, and Y. J. Guo, "Polarization Rotated Waveguide Antennas for Base Station Application," *IEEE Antenna and Propagation Letter*, vol. 16, pp. 1545-1548, Jan. 2017.

[30] J. Barrett, "5G Spectrum Bands," 2017. [Online]. Available: https://gsacom.com/5g-spectrum-bands/. [Accessed: 05-May-2019]

[31] S.-G. Zhou, P.-K. Tan, and T.-H. Chio, "Low-profile, wideband dualpolarized antenna with high isolation and low cross polarization," *IEEE Antenna and Propagation Letter*, vol. 11, pp. 1032-1035, 2012.

[32] C. F. Ding, X. Y. Zhang, Y. Zhang, Y. M. Pan and Q. Xue, "Compact Broadband Dual-Polarized Filtering Dipole Antenna With High Selectivity for Base-Station Applications," *IEEE Transactions on Antennas and Propagation*, vol. 66, no. 11, pp. 5747-5756, Nov. 2018.

[33] Y. Liu, S. Wang, N. Li, J. Wang and J. Zhao, "A Compact Dual-Band Dual-Polarized Antenna With Filtering Structures for Sub-6 GHz Base Station Applications," *IEEE Antennas and Wireless Propagation Letters*, vol. 17, no. 10, pp. 1764-1768, Oct. 2018.

[34] H. H. Sun, C. Ding, H. Zhu, and Y. J. Guo, "Suppression of Cross-Band Scattering in Multiband Antenna Arrays," *IEEE Transactions on Antennas and Propagation*, vol. 67, no. 4, pp. 2379-2389, Apr. 2019.

[35] H. H. Sun, H. Zhu, C. Ding, and Y. J. Guo, "Wideband Planarized Dual-Linearly-Polarized Dipole Antenna and Its Integration for Dual-Circularly-Polarized Radiation," *IEEE Antenna and Propagation Letter*, vol. 17, no. 12, pp. 2289-2293, Dec. 2018.

[36] HUBER+SUHNER, " DATA SHEET Coaxial Cable: ENVIROFLEX-316," 2008. [Online]. Available: http://www.inexim.pl/Download/Karty%20katalogowe%20RF/Kable/Enviroflex/ENVIROFLEX_316_dataSheet.pdf [Accessed: 05-May-2019]

Can Ding (M'16) was born in Anhui, China, in 1989. He received the Bachelor degree in Microelectronics from Xidian University, Xi'an, China, in 2009; and the PHD degree from Macquarie University, Sydney, Australia, in 2015. From 2012 to 2015, he is under the Cotutelle agreement between Macquarie University, Australia and Xidian University, China. During this period, he is also with Commonwealth Scientific and Industrial Research Organisation (CSIRO) DPaS Flagship, Marsfield, Australia.

From 2015 to 2017, he was a postdoctoral Research Fellow with the Global Big Data Technologies Centre (GBDTC), the University of Technology Sydney (UTS), Sydney, Australia, where he is currently a lecturer. His research interests include base station antennas, reconfigurable antennas, phase shifters, THz waveguides, and signal processing.

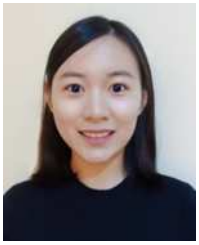

Haihan Sun was born in Shandong Province, China, in 1994. She received a Bachelor degree in Electronic Information Engineering from Beijing University of Posts and Telecommunications (BUPT), Beijing, China, in 2015; and a PhD degree in Engineering at the University of Technology Sydney (UTS), Sydney, Australia in 2019.

Her research interests include base station antennas and wideband omnidirectional antennas.

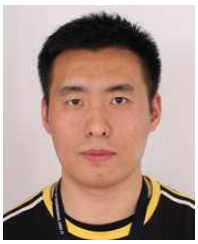

He Zhu (M'18) received the B.Sc degree and M.Eng degree from South China University of Technology, Guangzhou, China, and Ph.D. degree in Electrical Engineering from the School of ITEE, University of Queensland, Brisbane, Australia. He is currently a Post-doctoral Research Fellow with Global Big Data Technologies Centre (GBDTC), University of Technology Sydney (UTS), Australia.

His research interests include development of passive and tunable microwave and mm-wave devices, radio frequency integrated circuits and systems, and beam-forming networks for antenna arrays.

Y. Jay Guo (F'14) received a Bachelor Degree and a Master Degree from Xidian University in 1982 and 1984, respectively, and a PhD Degree from Xian Jiaotong University in 1987, all in China. His research interest includes antennas, mm-wave and THz communications and sensing systems as well as big data technologies. He has published over 450 research papers and holds 26 patents in antennas and wireless systems. He is a Fellow of the Australian Academy of Engineering and Technology, a Fellow of IEEE and a Fellow of IET, and was a member of the College of Experts of Australian Research Council (ARC, 2016-2018). He has won a number of most prestigious Australian engineering and CSIRO awards, and was named one of the most influential engineers in Australia in 2014 and 2015, respectively.

Prof Guo is a Distinguished Professor and the founding Director of Global Big Data Technologies Centre (GBDTC) at the University of Technology Sydney (UTS), Australia. Prior to this appointment in 2014, he served as a Director in CSIRO for over nine years, directing a number of ICT research portfolios. Before joining CSIRO, he held various senior technology leadership positions in Fujitsu, Siemens and NEC in the U.K.

Prof Guo has chaired numerous international conferences. He is the Chair Elect of International Steering Committee, International Symposium on Antennas and Propagation (ISAP). He was the International Advisory Committee Chair of IEEE VTC2017, General Chair of ISAP2015, iWAT2014 and WPMC'2014, and TPC Chair of 2010 IEEE WCNC, and 2012 and 2007 IEEE ISCIT. He served as Guest Editor of special issues on "*Antennas for Satellite Communications*" and "*Antennas and Propagation Aspects of 60-90GHz Wireless Communications*," both in IEEE Transactions on Antennas and Propagation, Special Issue on "*Communications Challenges and Dynamics for Unmanned Autonomous Vehicles*," IEEE Journal on Selected Areas in Communications (JSAC), and Special Issue on "*5G for Mission Critical Machine Communications*", IEEE Network Magazine.